CHAPTER 3

AlCoCrFeNi HIGH-ENTROPY ALLOY

This chapter illustrates the detailed study of synthesis and characterization of quinary equiatomic AlCoCrFeNi high-entropy alloy (HEA) prepared by mechanical alloying (MA). The dissolution of constituent elements and phase evolution with milling time has been followed systematically by X-ray diffraction (XRD) analysis. The variation of the morphology of powder particles with milling time has been studied through scanning electron microscopy (SEM). Transmission electron microscopy (TEM) was used to confirm the solid solution formation in the high-entropy alloy. The transformation of phases on the time-temperature scale has been investigated through differential scanning calorimetry (DSC), in-situ XRD and suitable heat-treatments. The microstructures of the microwave sintered compacts are characterized by optical microscopy and SEM.

3.1 Alloying behavior of elements and phase evolution

X-ray diffraction patterns of the mechanically alloyed powder of equiatomic AlCoCrFeNi high entropy alloy at different milling time has been given in Fig.3.1. Initially (0h of milling time) the diffraction peaks corresponding to all the constituent elements can be observed. As the milling time was increased, the peak intensity decreased dramatically. With the progress of milling time, the diffraction peaks corresponding to Co (d~ 2.20 Å (100) & 1.92Å (101)) and some higher angle peak of Al (d~ 1.22Å (311)) lose their identity after 5 h of milling time. It has been found that the elements other than the cubic structure of Fe & Cr start losing their signature earlier compared to the others. After 10 h of milling, the first peak of Al (d~ 2.33Å (111)) disappeared completely. This may be attributed to the lower melting (higher diffusivity)

temperature of Al that makes it possible to dissolve Al in the host lattice of Fe/Cr. As the milling time proceeds, more peaks were found to be disappearing. Noticeably, the disappearance of most of the elemental peaks indicated that complete solid solution phase has formed and closeness of the lattice parameter (2.89 ± 0.02 Å) of the alloy infers that Fe may be acting as a host lattice for this alloy.

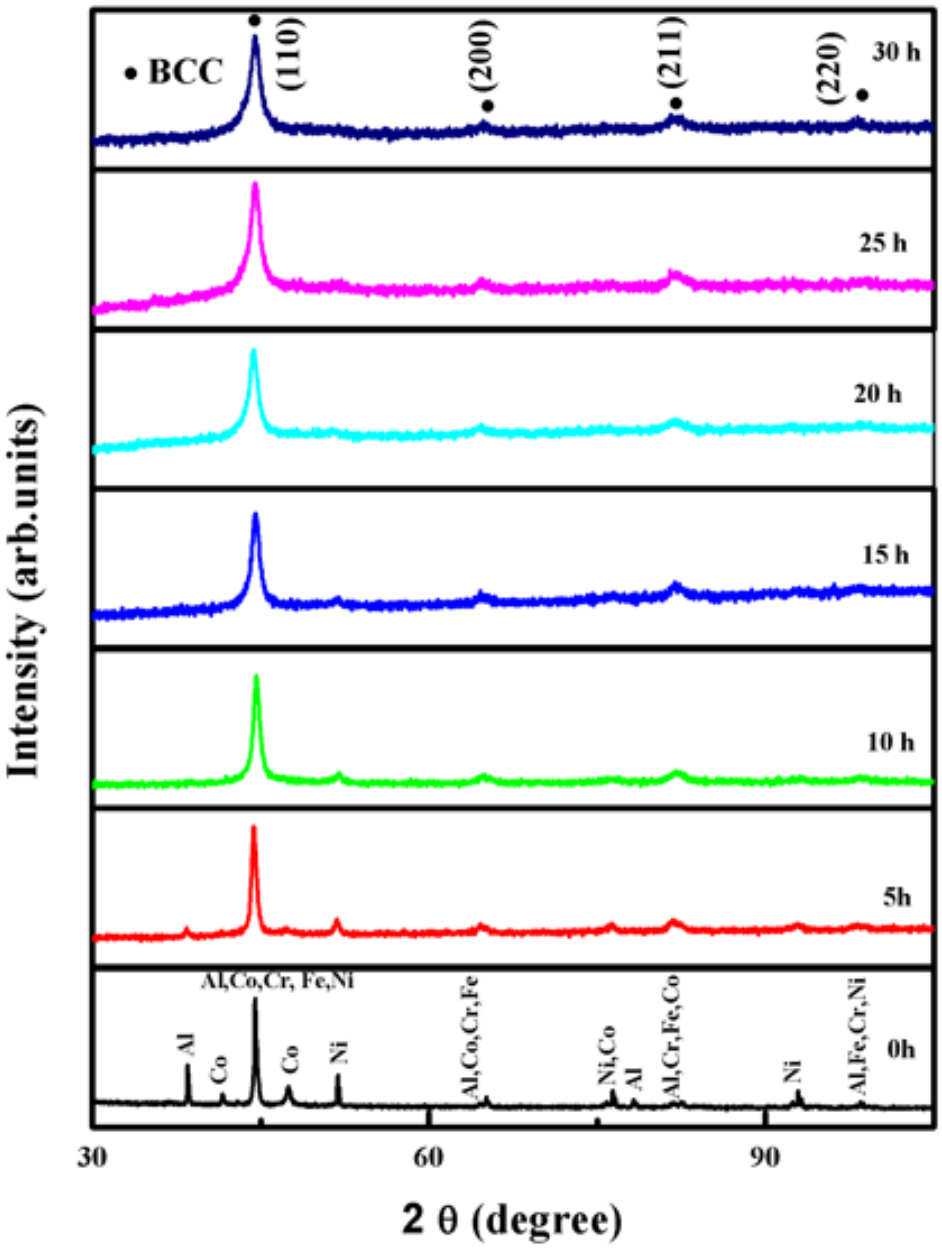

Figure 3.1: XRD patterns of AlCoCrFeNi HEA powders as a function of milling time. Evolution of a single-phase BCC structure was observed after 30 h of milling.

Although the solid solution phase was formed after 20 h of milling, it was carried out up to 30 h to get the more homogenized solid solution of finer grains and to track down any further milling induced changes in the alloy. It was also kept in mind that fine powder particles are more favourable for sintering [136]. The peak broadening and decrease in intensity throughout the diffraction pattern may be attributed to two main factors, i.e., high lattice strain and refined crystallite size [106,136].

Formation of a solid solution phase may mainly be attributed to the high entropy along with stronger bonding among constituent elements, atomic size difference, valence electron concentration and electronegativities of the atoms [49]. Primarily, a BCC solid solution phase with the cell parameter, 2.89 ± 0.02 Å close to that of BCC Fe was observed after 30 h of milling. The crystallite size (CS) and milling induced lattice strain during milling time were calculated by Scherrer's formula and Williamson-Hall method. The calculated results are listed in Table 3.1.

Table 3.1: The crystallite size and lattice strain of equiatomic AlCoCrFeNi HEA powder with milling time.

Milling time (h)	**Crystallite size (nm)**	**Lattice strain (%)**
5	19	0.56
10	15	0.70
15	12	0.87
20	10	1.08
25	9	1.09
30	9	1.20

As milling continued, crystallite size started decreasing, i.e. from 19 nm (5h milling) to 10 nm in 20h of milling time. This could be due to strain hardening of powders during MA. Milling of the powders up to 30h did not lead to any significant refinement in the

crystallites. Variation of crystallite size and lattice strain with the milling time has been shown in Fig.3.2.

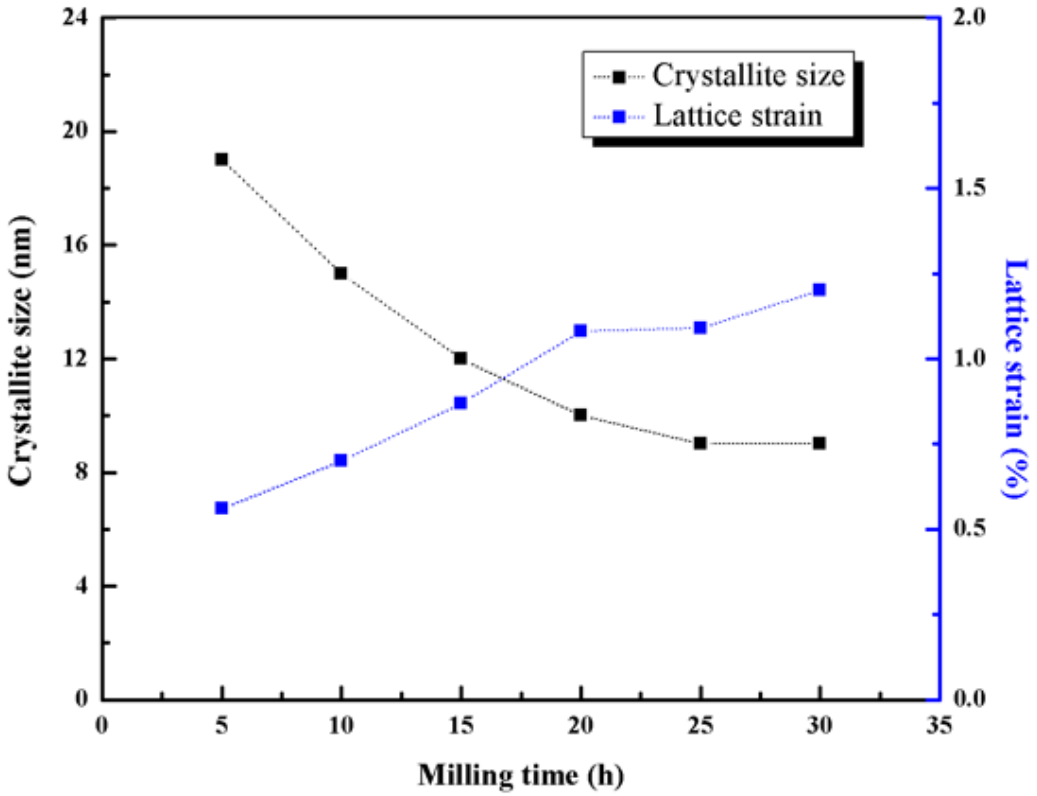

Figure 3.2: Variation of crystallite size and lattice strain has been shown as a function of milling time. It shows that crystallite size decreases with increases in lattice strain as milling proceeds with time.

During 30 h of milling, it has been found that there is a slight shift in Bragg angle (44.38-44.51º) towards the right side for (110) plane. This shift in the Bragg angle resulted due to the high impact forces that are involved in the mechanical alloying process leading to the accumulation of residual stress. Moreover, for crystal with a small lattice parameter, little change in lattice spacing may result in a high strain value [105].

3.2 Analysis of powder morphology

The SEM micrographs of AlCoCrFeNi high-entropy alloy powder after 10, 20 and 30 h of milling are given in Fig.3.3 (a-f) respectively. It is observed from the images that the particles size reduces continuously with the increase in milling time. Initially, the particles are faceted with a prominent river-like pattern on the surfaces, which is indicative of heavy deformation and fracturing. At the later stages of milling, flaky particles are also observed, and the volume fraction of flaky particles continuously increases. Probably, during the mechanical alloying process, continuous deformation, fracturing and cold welding lead to the enhanced diffusivity of the elements leading to the formation of HEA alloy. The evolutions of particle sizes with the milling time are given in Fig. 3.4. It appears that initially after 10 h of milling, the average particle size is ~10 μm and the range of particle size distribution spans over ~3-18 μm. However, with the progress of milling time, the average particle size reduces along with the reduction in the range of distribution of particle size. After 20 h of milling the average size and the range of distribution are ~8 μm and 3-17 μm respectively. The similar parameters after 30 h of milling are ~ 4 μm and 2-7 μm respectively. This observation necessarily means that the larger particles fractures first leading to a reduction in the average particle size and range of distribution and at the later stage, the fracture of the relatively finer particles takes place. During this time the particles also become alloyed. This indirectly helps in drawing the hypothesis that with particle fracturing relative surface area of the particle increases and the enhanced diffusivity at the particle surfaces helps in alloy formation.

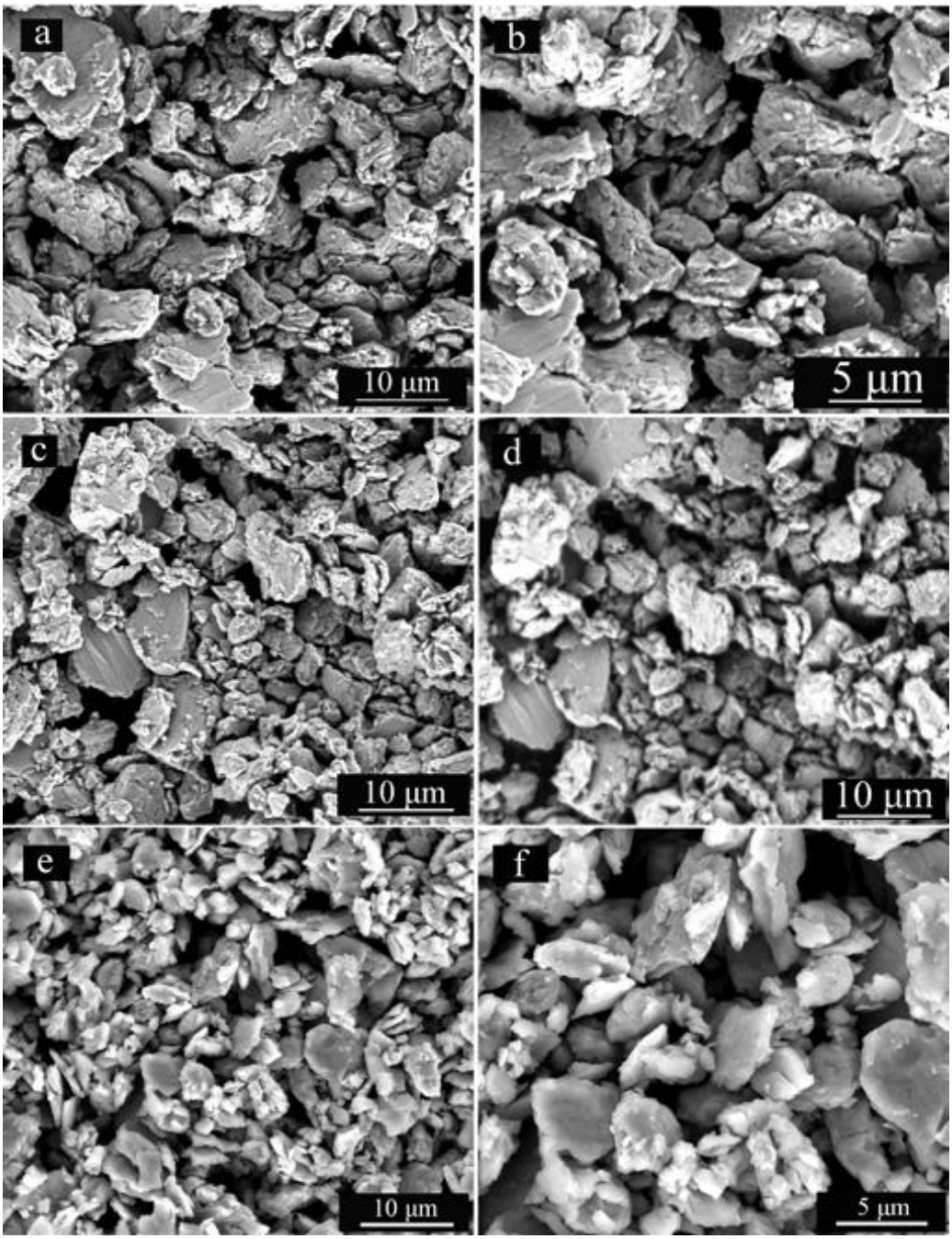

Figure 3.3: SEM micrographs of AlCoCrFeNi high-entropy alloy powder milled at 10 h (a&b) 20 h (c & d) and 30 h (e&f) for different magnifications. Particle sizes get reduced with the milling time.

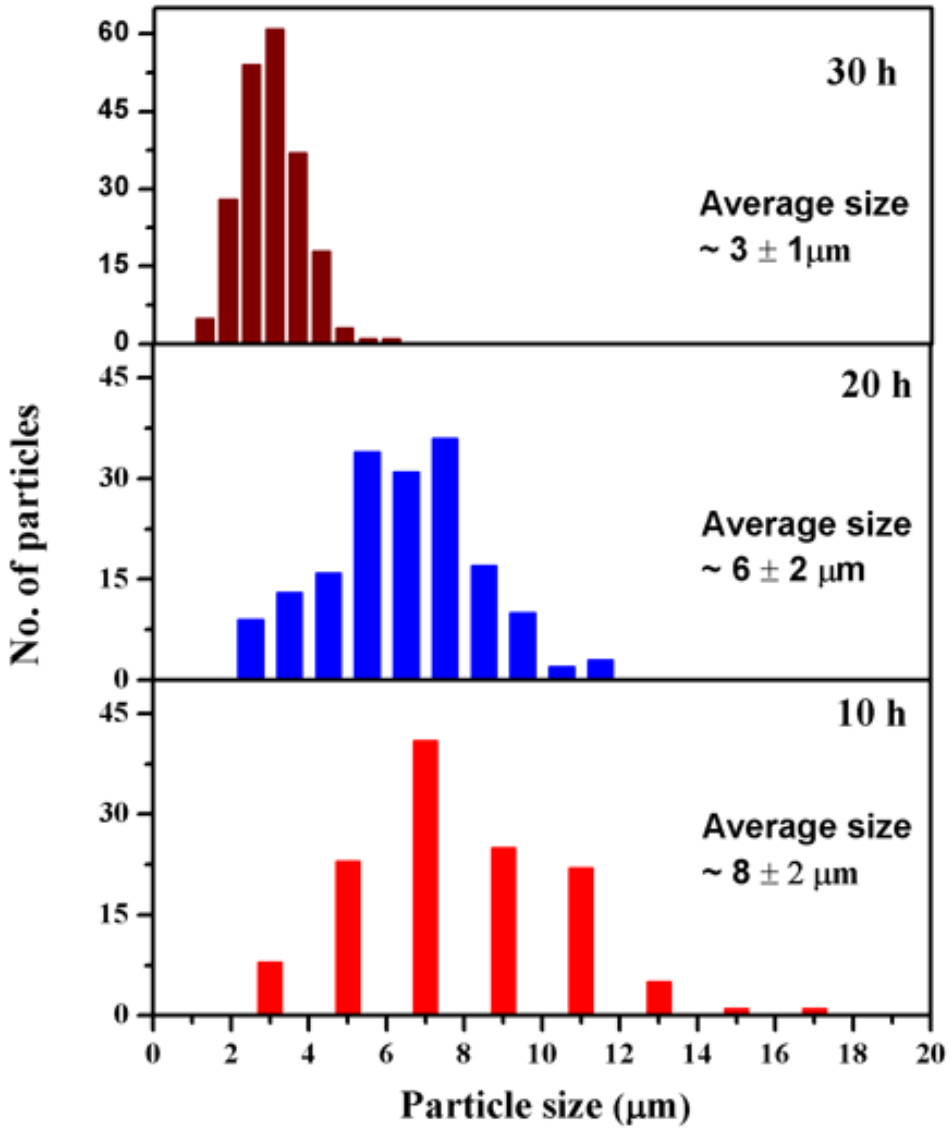

Figure 3.4: Distribution of particle sizes in AlCoCrFeNi high-entropy alloy with 10, 20 and 30 h of milling time. Reduction in the particle sizes was observed with progressive milling.

3.3 Nanostructured nature and phase evolution

The nanostructure of 30 h ball milled AlCoCrFeNi high-entropy alloy was confirmed by transmission electron microscopy (TEM). Bright-field and corresponding selected area diffraction (SAD) pattern have been shown in Fig.3.5. Formation of ring pattern in the SAD pattern indicates that the alloy particles are closely random distributed.

Indexing of the ring pattern confirmed the formation of a single-phase solid solution with BCC crystal structure (a= 2.89± 0.02Å). In the bright field image, the elongated or flaky morphology of the grains is observed. Additionally, in the image, irregular dark patches are present, which might be the remanence of residual strain that is present in the grain due to mechanical alloying.

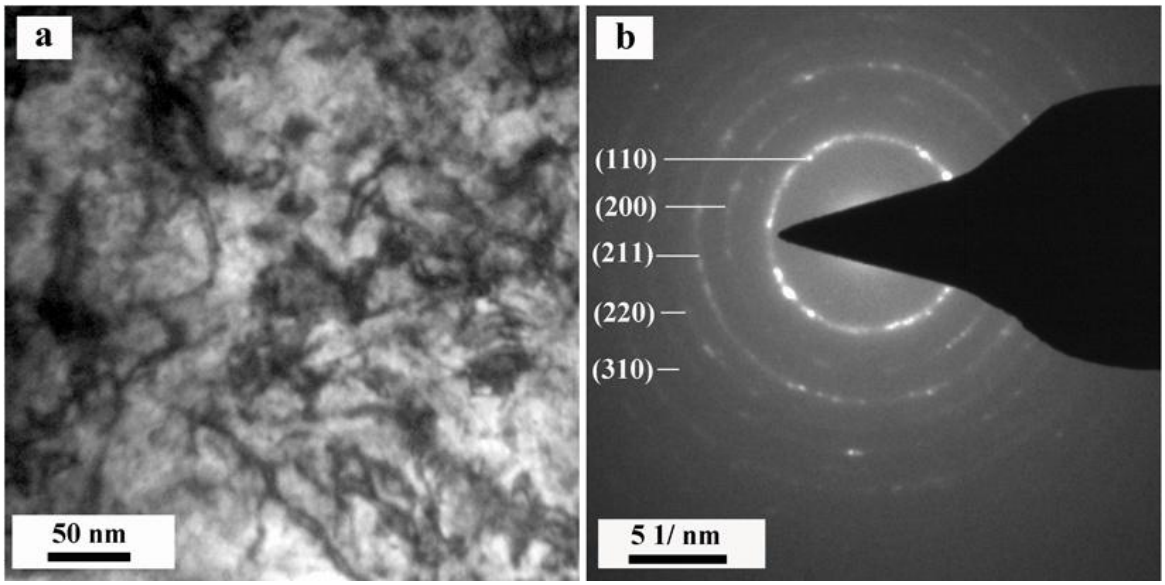

Figure 3.5: TEM images of AlCoCrFeNi high entropy alloy powder ball milled at 30h(a) Bright-field image, (b) Corresponding SAD pattern. Single-phase BCC structure can be confirmed by the diffraction pattern.

3.4 Thermal stability and phase evolution during heating

Thermal stability and phase evolution in this high entropy alloy was studied by differential scanning calorimetry (DSC). The differential scanning calorimetry thermogram over 300 ºC-1000 ºC (323-1273 K) temperature range with 40 K/min heating rate is given in **Fig. 3.6**. In the thermogram, prominent baseline shift is observed. The baseline shift at the initial stages of heating may be associated with thermal transients. At higher temperature also the baseline shift is present and only a small peak characterizing a phase change is observed at ~ 600 ºC (873 K). The heat evolution at this peak

temperature is not quite prominent, and thermal shift around the peak is also observed. It indicates that the alloy undergoes a diffusional transformation which does not have a strong characteristic temperature, rather it spans over a range of temperature. Due to the relatively high scanning rate thermal shift over a range of temperature is observed.

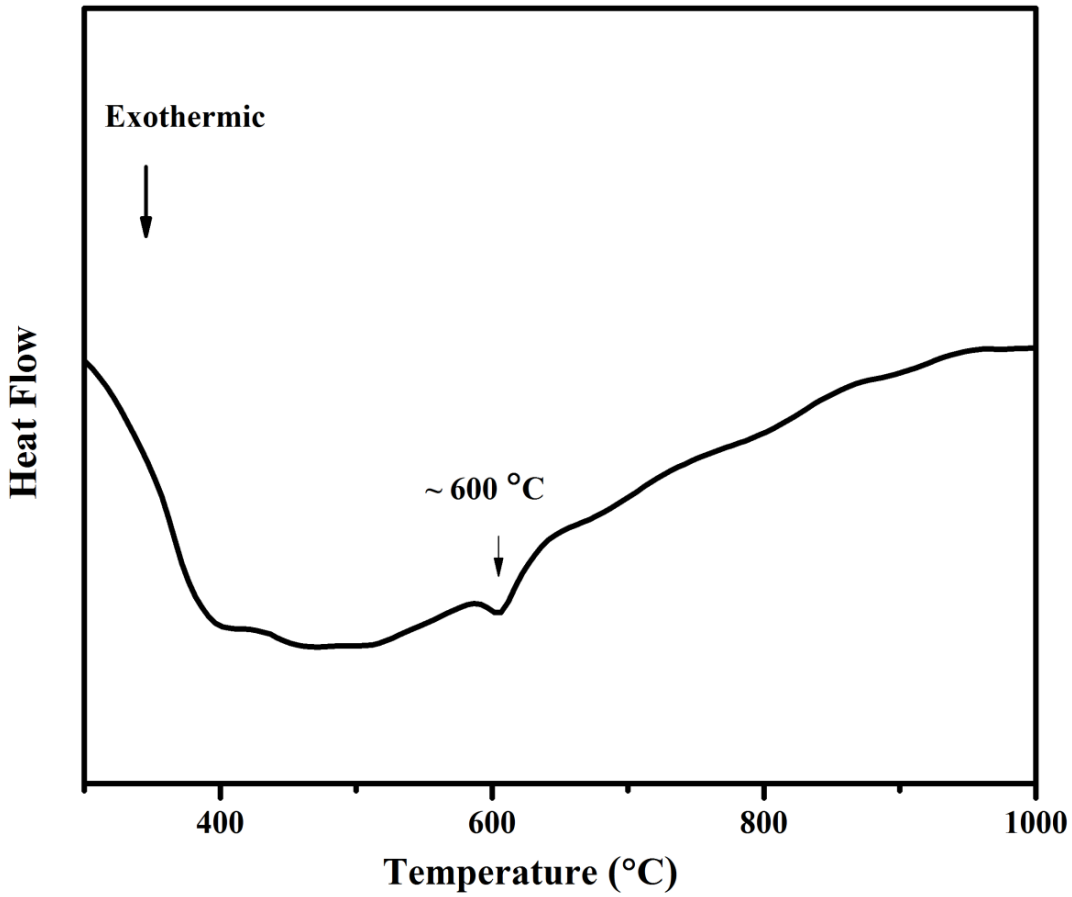

Figure 3.6: DSC thermogram of 30 h milled nanocrystalline equiatomic AlCoCrFeNi HEA heated upto 1000 ºC (1273K). Higher temperature small peak ~ 600 ºC (873K) indicates that alloy undergoes diffusion transformation which does not have a strong characteristic temperature.

It is also true that the alloy was synthesized by mechanical alloying, and the powder might have a lot of residual stress. The thermal shift may happen due to stress release from the material. However, the kinetics of stress release is not expected to be as fast to affect the baseline shift in the thermogram, especially when it is scanned at a faster rate.

In order to understand the diffusive nature of transformations in this high-entropy alloy over a wide range of temperature, the alloy was subjected to in-situ heating x-ray diffraction from room temperature to ~ 800 ºC (1073 K). Multiple displays of such diffraction patterns are given in Fig. 3.7. At room temperature, the diffraction peaks corresponding to the BCC phase as obtained after mechanical alloying is observed. However, as the sample is heated to 350 ºC (623 K), new peaks start appearing in the diffraction pattern which closely matches with the ordered Ni_3Al prototype $L1_2$ phase and ordered NiAl prototype B2 phase along with the initial BCC phase. It is understood that the B2 phase is an ordered version of the BCC phase. As the sample is heated through 425 ºC (698 K) up to 500 ºC (773K) similar peaks are observed in the diffraction pattern with little increase in their integrated intensities. However, at 575 ºC (848 K), apart from partially ordered B2 and $L1_2$ phases, some new peaks appear in the diffraction pattern, which can be indexed to Fe-Cr-Co type σ phase (tP30).

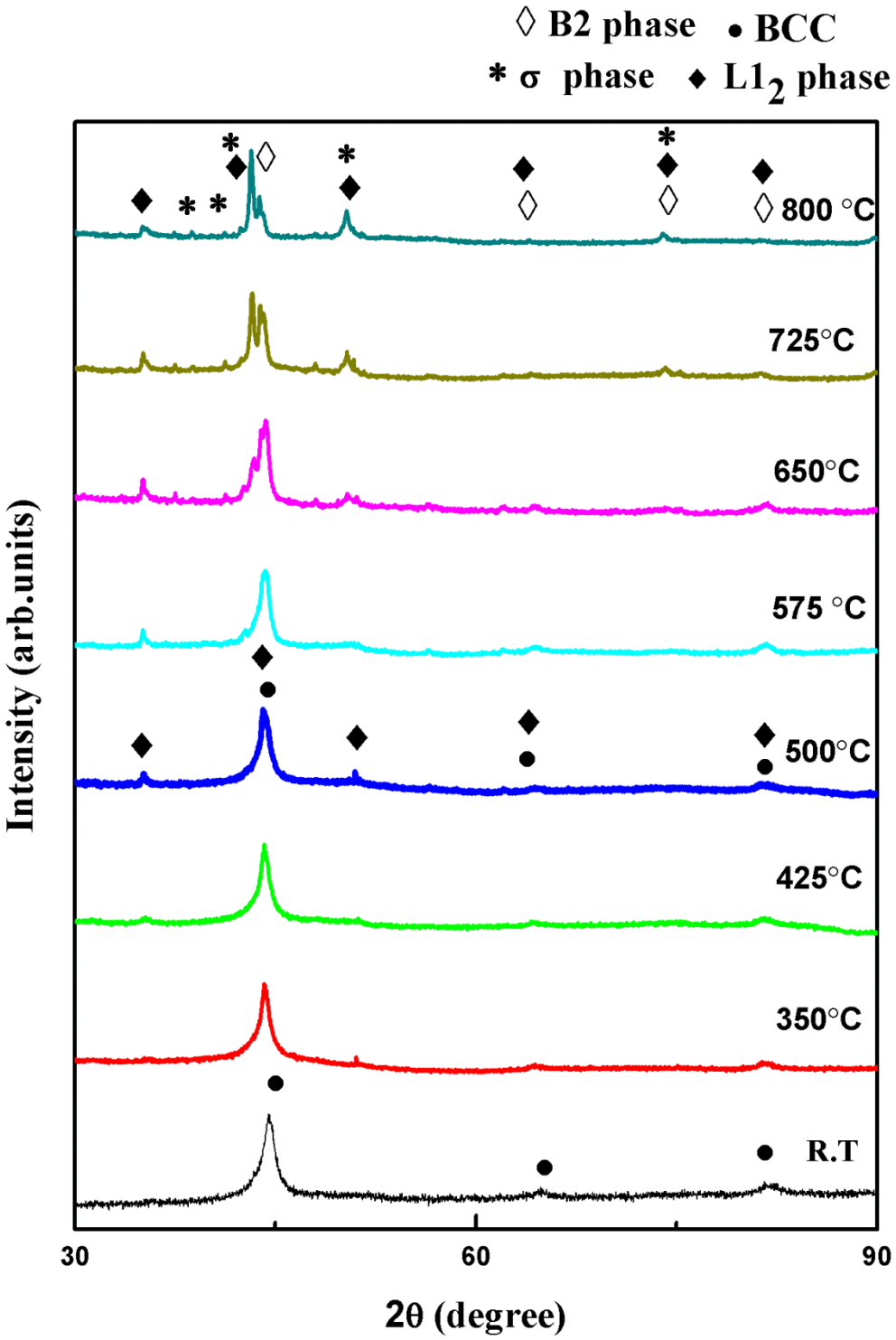

Figure 3.7: In-situ XRD plots of 30 h milled AlCoCrFeNi high entropy alloys powder upto 800ºC (1073K). Diffusive nature of phase transformation was evident even after 350 ºC (623K) and gets more support with an increase in temperature.

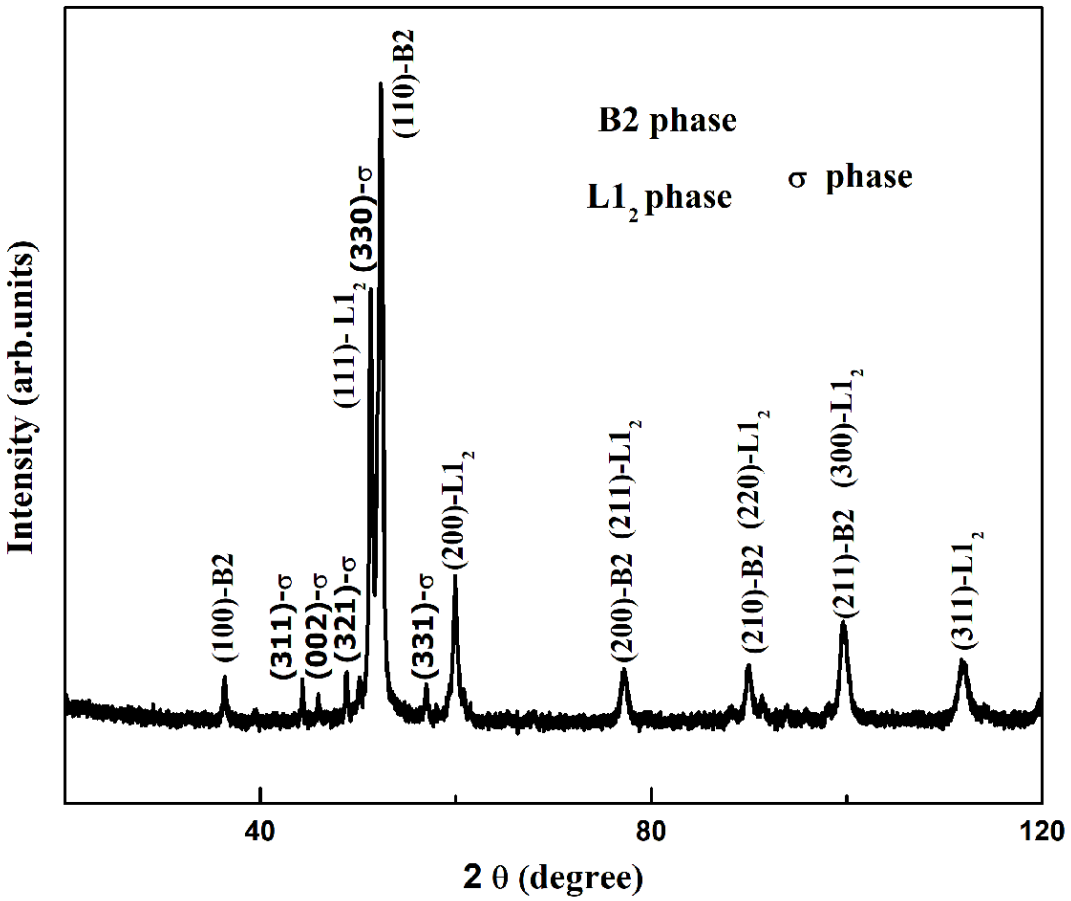

Figure 3.8: High-resolution XRD plot of the 30 h milled AlCoCrFeNi high entropy alloy powder after annealing for 1 h at 800ºC (1073K).

Even though the phase appears to evolve at this temperature, the intensities are quite weak. While heating through the higher temperatures i.e. at 650 ºC (923K), 725 ºC (998 K) and 800 ºC (1073 K), the peaks of σ phase becomes increasingly prominent and at 800 ºC (1073 K), almost all the major peaks of σ phase are present in the diffraction pattern along with the B2 and $L1_2$ phases. The experiment could not be conducted beyond that temperature. The as-synthesized high entropy alloy was vacuum annealed at 800 ºC for 1h and scanned by high-resolution XRD with Co-Kα radiation. The XRD scan is given in Fig.3.8. In this figure, the (100) and (210) peaks for ordered B2 phase are clearly observed. These peaks are not present for the as-synthesized disordered BCC high

entropy alloy. As order-disorder transformation is also diffusion-controlled and in the presence of so many elements kinetics for such transformation is likely to be slow, it is believed that only a certain fraction of disordered BCC unit cells transformed to ordered B2 phase leading to an overall partially disordered B2 phase.

3.5 Phase and microstructure evolution of the sintered alloy

XRD pattern of AlCoCrFeNi high entropy alloy after microwave sintering at 900 ºC (1173 K) along with the as-synthesized alloy have been displayed in Fig.3.9. In the as-synthesized alloy similar diffraction peaks as is given in Fig.3.1 are observed. However, after pelletization and sintering, a large number of new peaks are observed. Careful indexing of the peaks reveal the presence of the initial BCC phase as was obtained after mechanical alloying along with the peaks corresponding to Ni_3Al prototype $L1_2$ (a=3.58 ± 0.05 Å), NiAl prototype B2 (a=2.87 ± 0.02 Å) and Fe-Cr-Co (a=8.8 Å and c = 4.53 Å) based σ-phases. The phase evolution remains similar after microwave sintering. The point to be noted here is that during the in-situ high-temperature x-ray diffraction experiment, similar phases appeared at a much lower temperature.

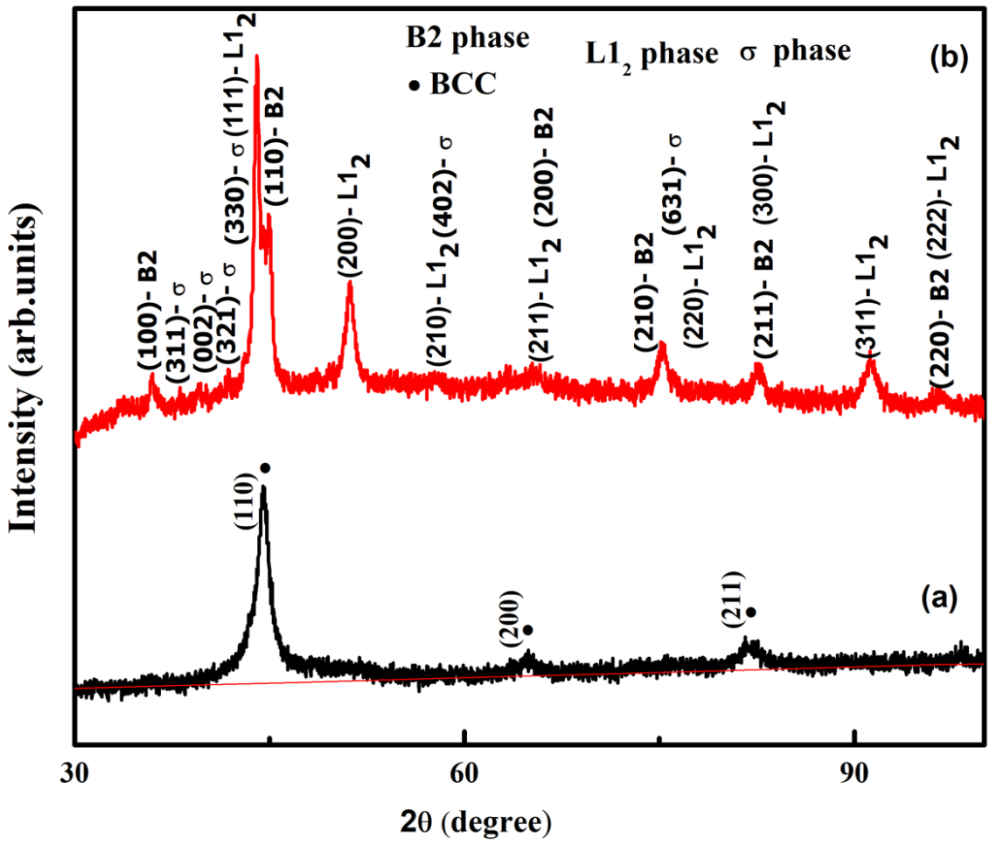

Figure 3.9: XRD pattern of AlCoCrFeNi high entropy alloy (a) synthesized powder of 30 h milling (b) microwave sintered pellet at 900 ºC (1173K), revealing the similar phase evolution as were observed in the in-situ XRD plot.

It will be discussed later in terms of thermal stability and microstructure evolution in this alloy. Fig. 3.10 shows the optical micrographs of microwave sintered alloy at 900 ºC (1173 K) at two different magnifications. It could be observed that the microstructure is uniform with the presence of some porosity.

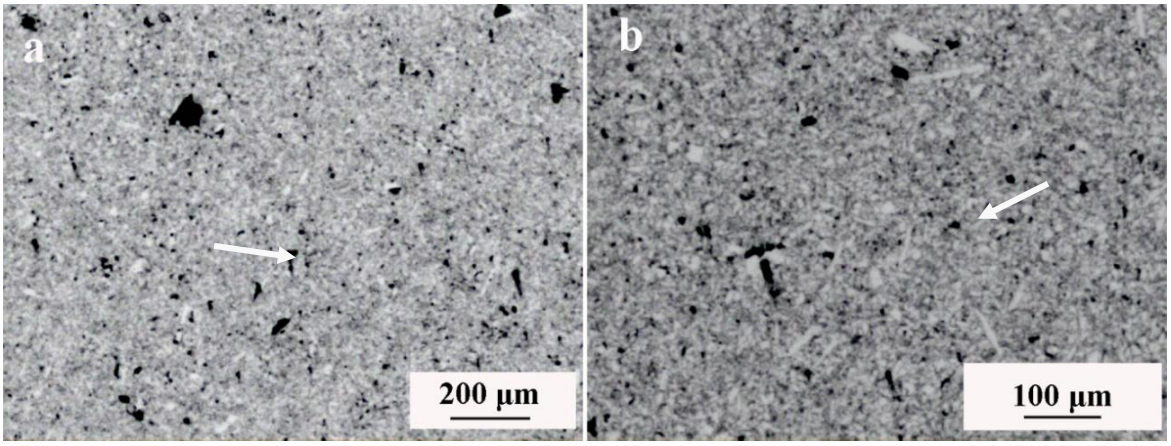

Figure 3.10: The optical microstructure of microwave sintered pellet at 900 ºC (1173K). (Porosity marked with arrows)

The SEM micrographs of microwave sintered samples at 800 ºC (1073K), 850 ºC (1123K) & 900 ºC (1173 K) for 1h have been shown in Fig.3.11 &3.12. In both the micrographs, the wide range of distribution of grain size is observed. After sintering, one set of grains are faceted, and another set of grains are fine and distributed in between the coarse grains.

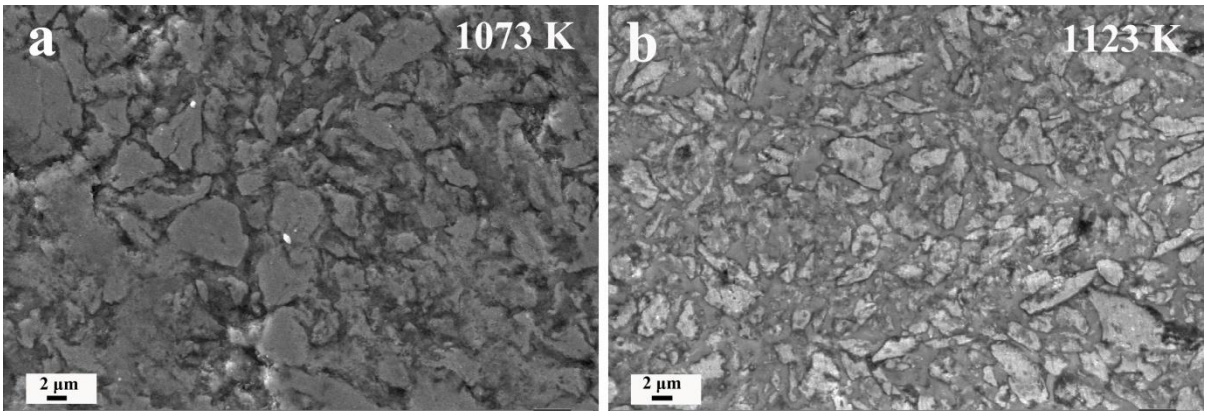

Figure 3.11: SEM micrographs of microwave sintered pellet at 800 ºC (1073K) & 850ºC (1123K).

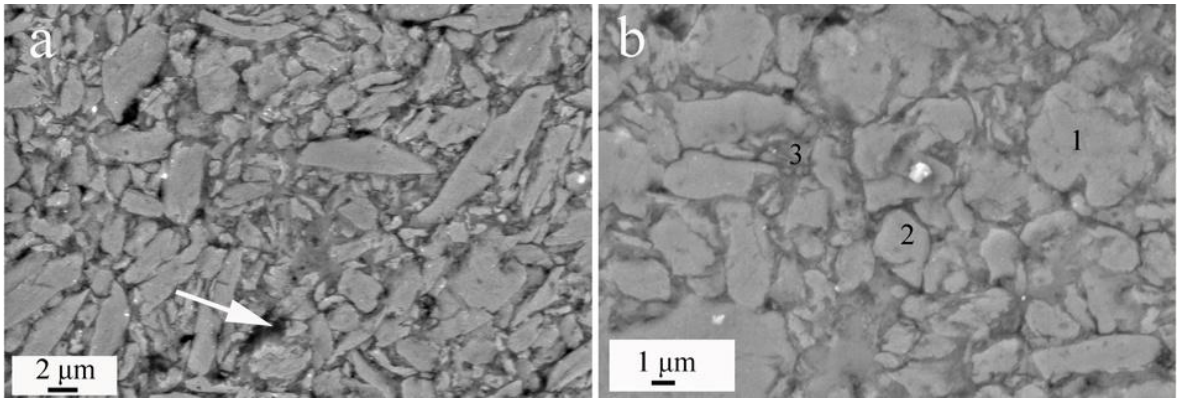

Figure 3.12: SEM micrographs of microwave sintered pellet at 900 ºC (1173K) revealing the wide distribution of grains of different sizes. Wider grain boundaries may be attributed to the diffusion assisted liquid phase sintering.

The size of the coarse grains is in the range of ~10-20 μm and that of the fine grains is in the range of ~ 0.5-2 μm. The interesting feature is that sharply defined grain boundaries are seen neither between the coarse grains nor between the fine grains. Rather the inter-granular spacing is quite wide approximately in the range of 1-1.5 μm. The wide inter-granular spacings may indicate diffusion assisted liquid phase sintering of the alloy. In the sintered microstructure, randomly distributed pores of irregular sizes are observed. The pores are ~ 0.5 - 1 μm of size and they are located at the grain interfaces. The pores might have originated due to its presence in the green compact or due to the shrinkage of the liquid phase at the inter-granular spacings while cooling of the sintered compact from the sintering temperature. X-ray energy dispersive spectroscopy in the point probe mode was done on the sintered samples at different points. The points are marked in the micrograph. The spectroscopy data are provided in Table 3.2. It can be understood that point 1 and point 2 are located on the coarse grain, and point 3 is located on the fine grain. It is observed from the data set that the ratio of (Ni, Fe, Co) to (Al, Cr) is ~ 3:1 which is very close to the Ni_3Al prototype $L1_2$ phase and that the same ratio in the fine grain is ~1:1 which might be considered as NiAl prototype B2 phase.

Table 3.2: SEM-EDX results of equiatomic AlCoCrFeNi high-entropy alloy**.**

Condition	Phases	Al (at. %)	Co (at. %)	Cr (at. %)	Fe (at. %)	Ni (at. %)
Microwave sintered	1	15.67	20.54	18.95	22.28	22.55
	2	17.79	16.45	15.04	26.51	24.21
	3	27.44	17.81	17.91	22.98	13.85

In other words, the composition from the fine and the coarse particles may be interpreted as an almost equiatomic composition with minor variation from perfect stoichiometry. However, Fe, Co, Ni, Al, Cr being very close to each other in the periodic table, a huge difference in the x-ray generation capability is not expected. Therefore, the variation in the chemistry of the particles could be attributed to the diffusion-assisted change in the chemistry of the particles during sintering, which results in the evolution of related phases in the microstructure. This observation also corroborates with the results obtained through in-situ high-temperature x-ray diffraction results.

3.6 Density measurement

The theoretical density of the sintered samples was calculated by applying the rule of mixture, using theoretical densities of the individual elements. The relative density of the samples was calculated by taking the ratio of measured and theoretical densities. It has been found that the relative density of the two samples was 81.48 % and 82.20 % respectively. It can be concluded from this study that the simultaneous application of pressure and temperature during sintering would lead to better density in the alloy. Microwave sintering can be used as an alternative technique for sintering of high-entropy alloy materials.

3.7 Discussion

It has been mentioned earlier that high-entropy alloys are of recent vintage in the family of multicomponent alloys. Even though the equiatomic AlCoCrFeNi high-entropy alloy has been reported and scattered data on its thermodynamics of formation, phase evolution and microstructure formation after sintering are available in the literature, in this study, its phase evolution, thermal stability, nature of transformation and microstructure evolution after microwave sintering has been studied systematically. Several observations which add to the further understanding should be discussed in detail in the light of currently available literature.

3.7.1 Alloy formation, phase evolution and HEA forming ability

The AlCoCrFeNi quinary equiatomic high-entropy alloy has been synthesized by different processing techniques, and it has been reported in the earlier literature [81]. Most important processing techniques are solidification, followed by casting and mechanical alloying followed by compaction and different methods of sintering [108]. The average atomic size difference of the constituent elements in this alloy is 5.72% (δ), which is a quite favourable value for substitutional solid solution formation. As the atomic size difference is not very high, and within the limit of Hume-Rothery rule of solid solution formation, it is expected on an empirical basis that this alloy would form solid solution upon alloying. The enthalpy of mixing (ΔH_{mix}) of the constituents as calculated from the Miedema model is -13.04 kJ/mol, and that of the configurational entropy (ΔS_{conf}) is 13.38 J/mol-K. These thermodynamic parameters such as $\Delta H_{mix,}$ ΔS_{conf}, δ and Ω are calculated based on the thermodynamic equation those are reported in chapter 1. The results of these calculations are compiled in Table 3.3.

Table 3.3: Calculated thermodynamic parameters for AlCoCrFeNi high entropy alloy.

ΔH_{mix} $\left(kJ/mol\right)$	δ (%)	ΔS_{conf} $\left(\frac{JK^{-1}}{mol}\right)$	Ω
-13.0442	5.727	13.38	1.83

A comparative look at the literature indicates that similar values have been reported for this alloy system [80]. However, the values calculated and reported by several groups vary slightly. It is believed that the source of data, approximation strategies etc. are different for different groups leading to the result in slightly differing values. It is important to evolve a unified approach to calculate the thermodynamic parameters in order to develop computational strategies to understand alloy formation, phase stability and microstructure evolution. The above-mentioned thermodynamic parameters are quite favourable for high-entropy alloy formation. The average atomic size difference being low, will not introduce large strain in the lattice upon substitution and enthalpy of mixing not being highly negative will not promote intermetallic phase formation. Additionally, it has been observed that the binary heat of mixing of different constituent elements (reported in Table 3.4) is not highly negative except Al-Ni, Al-Co and Co-Cr pairs. Should binary intermetallic phase formation in these three pairs is suppressed by some nonequilibrium method, high entropy solid solution phase is expected The calculated Ω parameter for this alloy is 1.83, which is again within the prescribed limit as reported in the earlier literature [35].

Table 3.4: The values of chemical mixing enthalpy, ΔH_{mix} (kJ/mol), of atomic pairs between elements for AlCoCrFeNi high entropy alloy.

Elements	Al	Co	Cr	Fe	Ni
Al	-	-19	-10	-11	-22
Co	-19	-	- 4	-1	0
Cr	- 10	- 4	-	-1	-7
Fe	- 11	- 1	- 1	-	-2
Ni	- 22	0	- 7	- 2	-

In the present study, after 30 hours of milling, a single BCC phase with a= 2.89 ± 0.02 Å has been obtained by X-ray and electron diffraction study. Some of the earlier studies on the same equiatomic composition have reported the formation of a BCC phase with same lattice parameter along with a FCC phase with 3.56 Å lattice parameter [80]. In the present work, the formation of any separate FCC phase could not be ascertained based on the x-ray and electron diffraction results. One of the important factors could be the metastable nature of the alloy, which leads to the formation of different phase composition due to slightly varying processing conditions. The metastable nature of this alloy and its influence on phase evolution would be discussed latter part of this chapter.

3.7.2 Thermal stability

It has been mentioned earlier that high-entropy alloy in equiatomic AlCoCrFeNi system has been reported earlier [137]. Several other alloy systems with very close similarity in terms of composition and constituents have also been reported [109,138]. As all of them form a single-phase solid solution or a two-phase solid solution, it is unanimously accepted to be high entropy phase. However, their thermal stability and the evolution of high entropy phases upon heat exposure are relatively less discussed and less understood. In the present alloy system, single-phase BCC structure was obtained upon

mechanical alloying. While dynamic heating in a differential scanning calorimeter (DSC) a diffused exothermic heat event was observed over a broad temperature range. This necessarily means that the alloy is metastable and it results in a number of phases upon heating. In-situ x-ray diffraction studies indicate that the BCC high entropy phase decomposes to give rise to Ni_3Al prototype $L1_2$ phase (a=3.57 Å) at a temperature as low as 425 ºC (698 K). Upon further heating, the NiAl prototype B2 (a=2.87 Å) phase appears and at the last stage of heating the σ-phase (tP30) is observed. It is worth mentioning that the B2 phase has a lattice parameter very close to the parent high entropy BCC phase. It can be postulated that the B2 phase and the high entropy phase are not completely uncorrelated; rather, it might be a derivative of parent high entropy BCC phase evolved through solute rejection and ordering. It is understood that the parent high-entropy BCC phase has all the elements where BCC Fe acts as the host lattice as the lattice parameter of the high entropy phase is very close to BCC Fe. Upon heating, Ni_3Al prototype $L1_2$ phase appears where Co & Fe may also be present along with Ni through the mechanism of substitution. This transformation leaves behind solute depleted parent BCC phase, which might resemble after the B2 phase in partially ordered or disordered form. Finally, rejection of Cr and its affinity towards Co, Fe may lead to the formation of the σ-phase. The complete transformation sequence may be represented schematically as follows;-

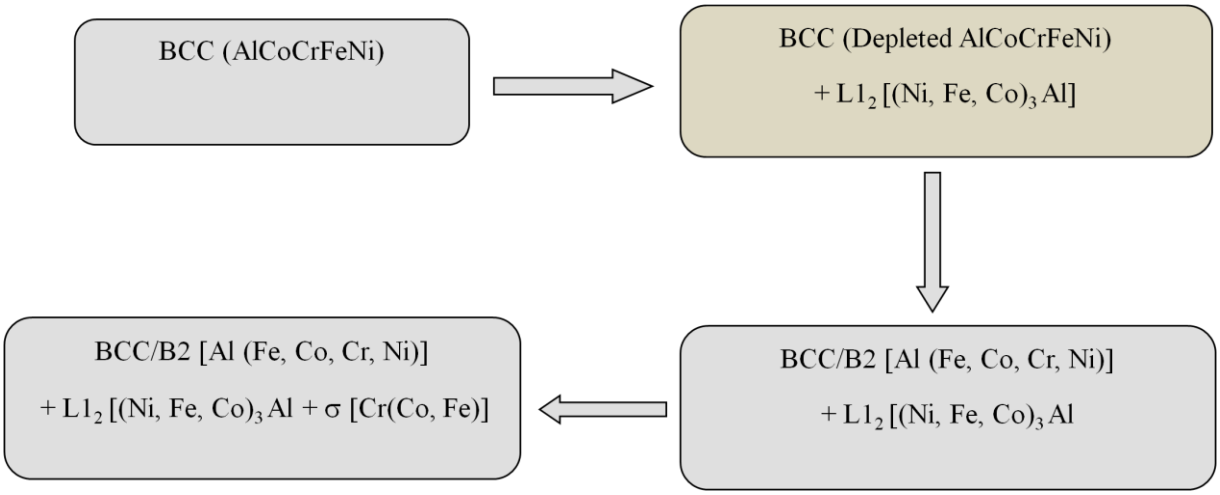

From the nature of the DSC thermogram, it appears that the transformation/precipitation of these phases takes place by the long-range diffusional transformation. However, as solute is rejected from the parent high entropy BCC phase, its solute content decreases and the precipitated phases are not high entropy phases in the strict sense of the term. Therefore, the high entropy nature of the alloy drifts from its original nature. Similar phases have been observed to be precipitated after microwave sintering and after spark plasma sintering, which was carried out at a much higher temperature. From the nature of the thermogram and precipitation of similar phases in a wide temperature range, it further confirms the diffusive nature of the transformation process. At this point, it is difficult to ascertain the absolute temperature of the transformation of this alloy.

Thermal stability of multicomponent high entropy alloys is in stark difference with the multicomponent bulk metallic glass-forming alloys. Most of the multicomponent bulk metallic glass-forming alloys show temperature defined transitions, e.g. glass transition temperature, crystallization onset temperature, subsequent transformation temperatures and melting temperature. Based on these temperature-defined transitions, several glass-forming ability criteria have evolved. Additionally, the glass transition temperature and the crystallization temperature signify the thermal stability of the glass-forming alloy

against crystallization. In this light, microstructural design for optimal properties has been easy. However, in this high-entropy alloy, such temperature defined transitions do not exist, which appears to be an impending difficulty in microstructure design in this alloy. Through in-situ high-temperature x-ray diffraction studies, it has been observed that the alloy starts transforming at a temperature as low as 350 ºC (623K), whereas similar phases are found to be precipitating during microwave sintering at 900 ºC (1173K) and at a still higher temperature during the spark plasma sintering process.

3.7.3 Microstructure evolution and its stability

It has been mentioned in the earlier sections that the alloy of a single phase is not thermally stable, and it undergoes a diffusional phase transformation to give rise to new phases. In the sintered sample, also similar phases are observed, and the grain boundary regions are quite wide, which may be indicative of liquid phase formation during sintering. As the alloy is multicomponent, there is a finite possibility of melting point depression. Apart from this study, earlier authors have also reported eutectoid transformation, spinodal decomposition etc [80, 81]. In the light of the current work and earlier published work, we encountered a number of fundamental questions in terms of microstructure evolution and phase stability. Basu and Ranganathan [4] have reported earlier in the context of multicomponent bulk metallic glass-forming alloys that eventhough a good fraction of possible binary phase diagrams have been determined in classical thermodynamic approach, the fraction of ternary known phase diagram is meagre and the same fraction decays exponentially as the number of components increases. To the best of the understanding, there is no absolutely determined quinary phase diagram. Moreover, the representation of such phase diagrams is difficult for want of higher dimensional representation. In this light, the determination of the stable phases

and their compositions is almost impossible. It will require trial and error based experimentation unless suitable models are developed. First principle approach may become handy in this regard. Even though the DSC thermogram and the in-situ high-temperature x-ray studies indicate that the alloy undergoes diffusive transformation at higher temperatures. However, it is difficult to associate them with any particular thermodynamic reaction.

3.8 Conclusions

The following conclusions can be drawn from this chapter:-

1. Equiatomic AlCoCrFeNi HEA with a single-phase BCC (a=2.89 ± 0.02 Å) solid solution has been synthesized after 30h of mechanical alloying using high-energy ball mill.
2. The high-entropy alloy synthesized after milling is not thermally stable. It precipitates Ni_3Al prototype $L1_2$ phase at a temperature as low as 350 ºC. Upon further heating NiAl prototype, B2 phase and Fe-Cr-Co prototype σ-phase are precipitated.
3. The precipitation of intermetallic phases from the parent high entropy BCC phase is diffusive in nature. It may be worth pursuing to investigate whether the product phases lead to the characteristics of high entropy alloy or not.
4. Similar phases are observed after microwave sintering. Microwave-assisted sintering can be used as an alternative way of sintering high entropy alloys with desirable but controlled porosities.